Magnetic Transition and Structural Asymmetrization in the Ferromagnetic Compound $[\{Ni_2(Medpt)_2(N_3)_2\}(\mu\text{-}(1,1\text{-}N_3)_2)]$, an Example of a Dynamic Second-Order Jahn−Teller Effect

Albert Escuer,*,† Ramon Vicente,† Joan Ribas,† and Xavier Solans‡

Departament de Química Inorgànica, Universitat de Barcelona, Diagonal 647, 08028-Barcelona, Spain, and Departament de Cristal.lografia i Mineralogia, Universitat de Barcelona, Martí Franqués s/n, 08028-Barcelona, Spain

Received April 5, 1994[⊗]

The synthesis, characterization and properties of the dinuclear nickel(II) complexes $[\{Ni_2(Medpt)_2(N_3)_2\}(\mu\text{-}(1,1\text{-}N_3)_2)]$ (**1**), $[\{Ni_2(dpt)_2(N_3)_2\}(\mu\text{-}(1,1\text{-}N_3)_2)]$ (**2**) and $[\{Ni_2(dpt)_2(N_3)_2\}(\mu\text{-}(1,3\text{-}N_3)_2)]$ (**3**), in which Medpt is methylbis(3-aminopropyl)amine and dpt is bis(3-aminopropyl)amine are described. The magnetic susceptibility for all three compounds has been recorded between 300 and 4 K; **1** and **2** show strong ferromagnetic coupling, and **3** shows antiferromagnetic behavior. Compound **1** shows a magnetic transition between 150 and 120 K. The crystal structure of **1** has been solved at 293 K and, after cooling to 118.5 K, at 190.5(3) K. Complex **1** crystallizes in the triclinic system, space group $P\bar{1}$, with fw = 576.0, 293 K [190.5 K], a = 7.331(1) [7.303(2)] Å, b = 8.091(1) [8.056(2)] Å, c = 11.389(2) [11.310(3)] Å, α = 71.96(2) [71.89(3)]°, β = 83.92(1) [83.57(2)]°, γ = 73.07(1) [72.74(2)]°, V = 614.4(3) [603.8(5)] Å^3, Z = 1, R = 0.063 [0.067], and R_w = 0.064 [0.068]. The phase transition and the magnetic behavior of **1** are described as the result of a reversible second-order Jahn−Teller effect.

Introduction

The early magnetic studies on nickel(II)-pseudohalide polynuclear complexes were performed during the 1970s (dinuclear compounds in all cases, typically with double pseudohalide bridge), showing antiferromagnetic (AF) coupling for cyanato[1] and azido[2,3] ligands and ferromagnetic (FM) coupling for thiocyanato ligand.[4] For more than 10 years these kinds of ligands practically have not been used in magnetic studies with nickel(II), and only two AF azido dinuclear compounds have been structurally characterized[5] in this period. At present, there is a spectacular growth in this research field, showing a large variety in the nuclearity and/or magnetic properties of the new nickel(II)−pseudohalide compounds. In this way, the azido ligand has allowed the synthesis of new FM[6−9] and AF[10] dinuclear compounds, one FM tetranuclear[11] compound, AF and FM homogeneous chains,[12,13] AF alternating chains[14,15] and AF planes;[16] by using the cyanato ligand one FM dinuclear[17] compound and one FM homogeneous chain[18] have been reported; for the thiocyanato ligand new FM dinuclear[19] complexes and homogeneous chains[20] have been reported; and, finally, for the selenocyanato ligand the first dinuclear compound[21] (FM) has been crystallographically characterized.

From the magnetic point of view, the most interesting characteristic of these nickel−pseudohalide systems lies in the fact that the azido ligand is a very effective superexchange pathway (J values in the $-114/+45$ cm^{-1} range) in its two coordination modes, end-to-end, which always gives AF behavior, and end-on, which always gives ferromagnetic coupling. In contrast, for the remaining NCO^-, NCS^-, and $NCSe^-$ ligands, very low $|J|$ values have been observed for all the reported compounds. It is difficult to predict the sign of J for the end-

† Departament de Química Inorganica.
‡ Departament de Cristalolographia i Mineralogia.
⊗ Abstract published in *Advance ACS Abstracts,* March 1, 1995.

(1) Ginsberg, A. P.; Martin, R. L.; Brookes, R. W.; Sherwood, R. C. *Inorg. Chem.* **1972**, *11*, 2884.
(2) Duggan, D. M.; Hendrickson, D. N. *Inorg. Chem.* **1974**, *13*, 2929.
(3) Wagner, F.; Mocella, M. T.; D'Aniello, M. J.; Wang, A. H. J.; Barefield, E. K. *J. Am. Chem. Soc.* **1974**, *96*, 2625.
(4) Pierpont, C. G.; Hendrickson, D. N.; Duggan, D. M.; Wagner, F.; Barefield, E. K. *Inorg. Chem.* **1975**, *14*, 604.
(5) Chauduri, P.; Guttmann, M.; Ventur, D.; Wieghardt, K.; Nuber, B.; Weiss, J. *J. Chem. Soc., Chem. Commun.* **1985**, 1618.
(6) Rojo, T.; Lezama, L.; Cortés, R.; Mesa, J. L.; Arriortua, M. I.; Villeneuve, G. *J. Magn. Magn. Mater.* **1990**, *83*, 519.; Arriortua, M. I.; Cortés, R.; Lezama, L.; Rojo, T.; Solans, X.; Font-Bardia, M. *Inorg. Chim. Acta* **1990**, *174*, 263.
(7) Escuer, A.; Vicente, R.; Ribas, J. *J. Magn. Magn. Mater.* **1992**, *110*, 181.
(8) Cortés, R.; Ruiz de Larramendi, J. I.; Lezama, L.; Rojo, T.; Urtiaga, K.; Arriortua, M. I. *J. Chem. Soc., Dalton Trans.* **1992**, 2723.
(9) Vicente, R.; Escuer, A.; Ribas, J.; El Fallah, M. S.; Solans, X.; Font-Bardia, M. *Inorg. Chem.* **1993**, *32*, 1920.
(10) Ribas, J.; Monfort, M.; Diaz, C.; Bastos, C.; Solans, X. *Inorg. Chem.* **1993**, *32*, 3557.
(11) Ribas, J.; Monfort, M.; Costa, R.; Solans, X. *Inorg. Chem.* **1993**, *32*, 695.
(12) (a) Escuer, A.; Vicente, R.; Ribas, J.; El Fallah, M. S.; Solans, X. *Inorg. Chem.* **1993**, *32*, 1033. (b) Escuer, A.; Vicente, R.; Ribas, J.; El Fallah, M. S.; Solans, X.; Font-Bardia, M. *Inorg. Chem.* **1993**, *32*, 3727. (c) Vicente, R; Escuer, A.; Ribas, J.; El Fallah, M. S.; Solans, X.; Font-Bardia, M. *Inorg. Chem.*, in press.
(13) Ribas, J.; Monfort, M.; Diaz, C.; Bastos, C.; Solans, X. *Inorg. Chem.* **1994**, *33*, 484.
(14) (a) Vicente, R.; Escuer, A.; Ribas, J.; Solans, X. *Inorg. Chem.* **1992**, *31*, 1726. (b) Escuer, A.; Vicente, R.; Ribas, J.; El Fallah, M. S.; Solans, X.; Font-Bardia, M. *Inorg. Chem.* **1994**, *33*, 1842.
(15) Escuer, A.; Vicente, R.; El Fallah, M. S.; Ribas, J.; Solans, X.; Font-Bardia, M. *J. Chem. Soc. Dalton Trans.* **1993**, 2975.
(16) (a) Monfort, M.; Ribas, J.; Solans, X. *J. Chem. Soc., Chem. Commun.* **1993**, 350. (b) Ribas, J.; Monfort, M.; Solans, X.; Drillon, M. *Inorg. Chem.* **1994**, *33*, 742.
(17) Arriortua, M. I.; Cortés, R.; Mesa, J. L.; Lezama, L.; Rojo, T.; Villeneuve, G. *Transition Met. Chem.* **1988**, *13*, 371.
(18) Escuer, A.; Vicente, R.; Ribas, J.; El Fallah, M. S.; Solans, X.; Font-Bardia, M. *Inorg. Chim. Acta* **1994**, *216*, 5.
(19) Rojo, T.; Cortés, R.; Lezama, L.; Arriortua, M. I.; Urtiaga, K.; Villeneuve, G. *J. Chem. Soc., Dalton Trans.* **1991**, 1779.
(20) Vicente, R.; Escuer, A.; Ribas, J.; Solans, X. *J. Chem. Soc., Dalton Trans.* **1994**, 259.
(21) Vicente, R.; Escuer, A.; Ribas, J.; Solans, X.; Font-Bardia, M. *Inorg. Chem.* **1993**, *32*, 6117.

0020-1669/95/1334-1793$09.00/0

to-end cyanato ligand, whereas the systems with end-to-end thiocyanato and selenocyanato ligands are always ferromagnetically coupled.

Following with our research in this field, in this paper we explore the reactivity of the nickel(II)−open triazaamines−azido bridge system, using Medpt (bis(3-aminopropyl)methylamine) and dpt (bis(3-aminopropyl)amine) as blocking ligands for three sites of the coordination polyhedron of the nickel(II).

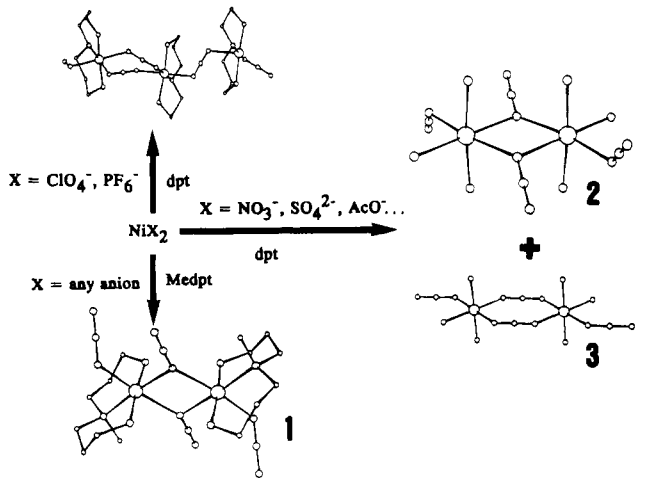

In a previous paper,[14] the first derivative of this system, the alternating chain with the unusual $\{-(N_3)-Ni(dpt)-(N_3)_2-Ni(dpt)-\}_n$ scheme, obtained by the reaction of nickel(II) perchlorate, dpt, and sodium azide was described. Reaction of any nickel salt with Medpt and sodium azide yields the dinuclear compound $[\{Ni_2(Medpt)_2(N_3)_2\}(\mu\text{-}(1,1\text{-}N_3)_2)]$ (**1**), in which the azido ligand shows end-on coordination, whereas reaction of any nickel salt (except the perchlorate and hexafluorophosphate), with dpt and sodium azide yields the two isomers of the dinuclear compound $[\{Ni_2(dpt)_2(N_3)_2\}(\mu\text{-}N_3)_2)]$, in which the azido ligand is coordinated in the end-on (**2**) or end-to-end (**3**) mode.

The main goal of this study is the characterization of compound **1**, which shows a magnetic transition around 150−120 K. This transition was seen to be a reversible phenomenon by susceptibility, calorimetric, and X-ray powder measurements, and finally it was fully characterized by means of the structural determination at 293 and 190.5 K (after cooling at 118.5 K). Experimental results are in full agreement with the assumption that the transition studied is due to a dynamic second-order Jahn−Teller effect, reversible in the room temperature−80 K range.

Experimental Section

Preparation of Complexes. Compound $[\{Ni_2(Medpt)_2(N_3)_2\}(\mu\text{-}(1,1\text{-}N_3)_2)]$ (**1**), was obtained by slow evaporation of aqueous solutions of any nickel(II) salt, Medpt, and sodium azide in stoichiometric amounts, giving well-formed blue crystals. Small amounts of nickel hydroxide should be removed before the addition of the sodium azide. Compounds $[\{Ni_2(dpt)_2(N_3)_2\}(\mu\text{-}N_3)_2)]$, **2** and **3**, were obtained in a similar way, by using any nickel(II) salt except perchlorate or hexafluorophosphate, in which case the 1D complexes $[\{Ni_2(dpt)_2(\mu\text{-}N_3)(\mu'\text{-}(N_3)_2\}_n]X_n$, X = ClO_4^- or PF_6^-, were obtained.[14] Slow evaporation of these aqueous solutions first gave compound **2** as small blue crystalline needles. Further evaporation of the remaining solution gave blue crystalline plates of **3**. Despite the crystallinity of **2** and **3**, all attempts to obtain crystals suitable for X-ray determination were unsuccessful.

It is interesting to point out that the synthesis of these complexes shows the influence of the nonbridging ligand and the counteranion in the coordination mode of the bridging azido groups: for **1** only the end-on coordination is stabilized with absolute independence of the anionic group present in solution. In contrast, the dpt amine gives three compounds depending on the counteranion (1D system using $Ni(ClO_4)_2{\cdot}6H_2O$[14] and both dinuclear coordination isomers **2** and **3** using Cl^-, SO_4^{2-}, AcO^- or NO_3^-).

These four compounds, with large structural and coordination differences, show the extreme versatility of the azido ligand. Moreover, it should be taken into account that, at present, the factors that induce the stability of a particular compound are not clear.

Table 1. Crystallographic Data for $[\{Ni_2(Medpt)_2(N_3)_2\}(\mu\text{-}(N_3)_2)]$, **1**, at 293 K and 190.5 K

	T = 293 K	T = 190.5 K	T = 118.5 K
formula	$C_{14}H_{38}N_{18}Ni_2$	$C_{14}H_{38}N_{18}Ni_2$	$C_{14}H_{38}N_{18}Ni_2$
a, Å	7.331(1)	7.303(2)	7.295(4)
b, Å	8.091(1)	8.056(2)	8.069(1)
c, Å	11.389(2)	11.310(3)	11.302(3)
α, deg	71.96(2)	71.89(3)	72.04(2)
β, deg	83.92(1)	83.57(2)	84.00(3)
γ, deg	73.07(1)	72.74(2)	72.44(1)
V, Å^3	614.4(3)	603.8(5)	603.3(6)
Z	1	1	1
fw	576.0	576.0	576.0
space group	$P\bar{1}$	$P\bar{1}$	$P\bar{1}$
temp, K	293	190.5	118.5
λ(Mo Kα), Å	0.710 69	0.710 69	0.710 69
d_{cal}, g·cm^{-3}	1.518	1.545	1.546
μ(Mo Kα), cm^{-1}	15.72	15.99	16.01
$R(F_o)^a$	0.063	0.067	
$R_w(F_o)^b$	0.064	0.068	

^{a} $R(F_o) = \sum||F_o| - |F_c||/\sum|F_o|$. ^{b} $R_w(F_o) = \sum w||F_o| - |F_c||/\sum w|F_o|$.

Physical Measurements. Infrared spectra (4000−200 cm^{-1}) were recorded from KBr pellets in a Perkin Elmer 1330 IR spectrophotometer. Electronic spectra were measured in a Shimadzu UV 160 A spectrophotometer, in the 1100−200 nm range. Magnetic measurements were carried out with a pendulum-type magnetometer (MANICS DSM8) equipped with a helium continuous-flow cryostat working in the temperature range 300−4 K, and a Brucker B-E15 electromagnet. The magnetic field was approximately 1.5 T. Diamagnetic corrections were estimated from Pascal tables. DSC measurements were carried out in a Perkin-Elmer DSC-7 differential scanning calorimeter with cryogenic equipment, using a cooling/heating rate of 5° min^{-1}. Powder X-ray diffraction data were collected with a Siemens D500 automated diffractometer, using a TTK Aaton-Par camera, Cu Kα radiation, and secondary monochromator.

Crystal Data Collection and Refinement. A prismatic crystal (0.1 × 0.1 × 0.2 mm) of **1** was selected and mounted on a Enraf-Nonius CAD4 diffractometer. The crystallographic data, conditions retained for the intensity data collection and some features of the structure refinement are listed in Table 1. The accurate unit-cell parameters were determined from automatic centering of 25 reflections ($12 \le \theta \le 16°$) and refined by least-squares method. Intensities were collected, first at 293 K, and after cooling to 118.5 K at which the cell-parameters where determined, the crystal was warmed to 190.5(3) K and a new set of data was collected. Graphite monochromatized Mo Kα radiation, with $\omega-2\theta$ scan technique, scan width 0.8° and scan speed 0.03° s^{-1} was used.

A total of 3624 (293 K) and 2150 (190.5 K) reflections were measured in the range $2 \le \theta \le 30°$ (293 K) and $2 \le \theta \le 25°$ (190.5 K). A total of 3236 (293 K) and 1956 (190.5 K) reflections were assumed as observed applying the condition $I \ge 2.5\sigma(I)$. In both cases, three reflections were measured every 2 h as orientation and intensity control, and significant intensity decay was not observed. Corrections were made for Lorentz−polarization but not for absorption. The high-temperature structure was solved by direct methods, using the SHELX86 computer program,[22] and the low-temperature structure was determined from the high-temperature data. Both structures were refined by a full-

(22) Sheldrick, G. M. *Acta Crystallogr.* 1990, *A46*, 467.

Table 2. Final Atomic Coordinates and Equivalent Isotropic Thermal Parameters (Å^2) and Their Estimated Standard Deviations for [{$Ni_2(Medpt)_2(N_3)_2$}(μ-$(N_3)_2$)], **1**, at 293 K

	x/a	y/b	z/c	B_{EQ}[a]
Ni(1)	0.02019(3)	0.47990(3)	0.35156(2)	1.58(2)
N(1)	0.1257(3)	0.6014(3)	0.4700(2)	1.96(8)
N(2)	0.2594(3)	0.6601(3)	0.4672(2)	2.11(7)
N(3)	0.3884(4)	0.7170(5)	0.4638(3)	3.61(12)
N(4)	−0.1138(4)	0.3543(3)	0.2657(2)	2.58(9)
N(5)	−0.1015(3)	0.1979(3)	0.2968(3)	2.68(9)
N(6)	−0.0929(5)	0.0453(4)	0.3258(5)	5.20(18)
N(7)	−0.2075(3)	0.7138(3)	0.3071(2)	2.02(8)
C(8)	−0.2823(4)	0.7876(4)	0.1805(3)	2.43(9)
C(9)	−0.1296(4)	0.8398(4)	0.0889(3)	2.80(10)
C(10)	0.0278(4)	0.6771(4)	0.0734(2)	2.48(9)
N(11)	0.1641(3)	0.5786(3)	0.1762(2)	1.97(7)
C(12)	0.2941(4)	0.4278(4)	0.1347(3)	2.79(10)
C(13)	0.4447(4)	0.2924(5)	0.2238(3)	3.16(11)
C(14)	0.3665(4)	0.1575(4)	0.3254(3)	2.75(10)
N(15)	0.2455(3)	0.2461(3)	0.4128(2)	2.25(8)
C(16)	0.2742(5)	0.6976(4)	0.1884(3)	2.95(11)

[a] $B_{EQ} = 8\pi^2/3\ \Sigma_i\Sigma_j U_{ij}\ a^*_j\ a^*_i\ a_i a_j$.

Table 3. Final Atomic Coordinates and Equivalent Isotropic Thermal Parameters (Å^2) and Their Estimated Standard Deviations for [{$Ni_2(Medpt)_2(N_3)_2$}(μ-$(N_3)_2$)], **1**, at 190.5 K

	x/a	y/b	z/c	B_{EQ}[a]
Ni(1)	0.02019(5)	0.48001(5)	0.35135(3)	0.91(3)
N(1)	0.1265(5)	0.6011(5)	0.4716(3)	1.29(13)
N(2)	0.2598(4)	0.6601(4)	0.4682(3)	1.19(12)
N(3)	0.3864(5)	0.7183(5)	0.4659(3)	2.11(14)
N(4)	−0.1148(5)	0.3547(5)	0.2637(3)	1.61(14)
N(5)	−0.0998(4)	0.1964(4)	0.2965(3)	1.56(13)
N(6)	−0.0876(6)	0.0429(5)	0.3259(4)	3.37(19)
N(7)	−0.2077(5)	0.7152(4)	0.3066(3)	1.24(12)
C(8)	−0.2859(5)	0.7900(5)	0.1794(3)	1.48(14)
C(9)	−0.1329(6)	0.8430(5)	0.0871(3)	1.84(15)
C(10)	0.0272(5)	0.6780(5)	0.0724(4)	1.58(15)
N(11)	0.1645(5)	0.5781(4)	0.1758(3)	1.20(12)
C(12)	0.2951(5)	0.4263(5)	0.1334(3)	1.66(15)
C(13)	0.4480(6)	0.2882(5)	0.2246(4)	2.06(16)
C(14)	0.3691(5)	0.1550(5)	0.3268(3)	1.59(14)
N(15)	0.2436(5)	0.2448(5)	0.4135(3)	1.37(13)
C(16)	0.2760(6)	0.6958(5)	0.1885(4)	1.73(15)

[a] $B_{EQ} = 8\pi^2/3\ \Sigma_i\Sigma_j U_{ij}\ a^*_j\ a^*_i\ a_i a_j$.

matrix least-squares method, using the SHELX76 computer program.[23] The function minimized was $\Sigma w[[F_o] - [F_c]]^2$, where $w = (\sigma^2(F_o) + k[F_o]^2)^{-1}$ and where $k = 0.0078$ (293 K) and 0.0150 (190.5 K). f, f', and f'' were taken from ref 24. The position of 17 H atoms was obtained from a difference synthesis and refined with an overall isotropic temperature factor, using a riding model for 16 H atoms. The final R factor was 0.063 ($R_w = 0.064$) (293 K) and 0.067 ($R_w = 0.068$) (190.5 K). Number of parameters refined = 161. Maximum shift/esd = 0.1; Maximum and minimum peaks in the final difference synthesis were 0.3 and −0.3 e Å^{-3}, respectively in both structures. Final atomic coordinates are given in Tables 2 and 3. Selected bond lengths and angles are given in Table 4 and a labeled schema is shown in Figure 1.

Results

IR and Electronic Spectra. The $\nu_{as}(N_3)$ band is centered at 2020 cm^{-1} for all three compounds, as a very intense and broad absorption. The $\nu_s(N_3)$ band could be expected at 1300 cm^{-1}, but this region is obscured by the amine characteristic bands. The δ azide bending can be observed at 605−615 cm^{-1} for compounds **1** and **2**, whereas for **3** it appears at 635−645 cm^{-1}. Characteristic bands of the amine and perchlorate groups appear at normal frequencies. Electronic spectra in aqueous solution are typical of hexacoordinate nickel(II) systems, showing three absorptions centered at 970, 604, and 367 nm for **1** and **2** and 991, 611, and 373 nm for **3**.

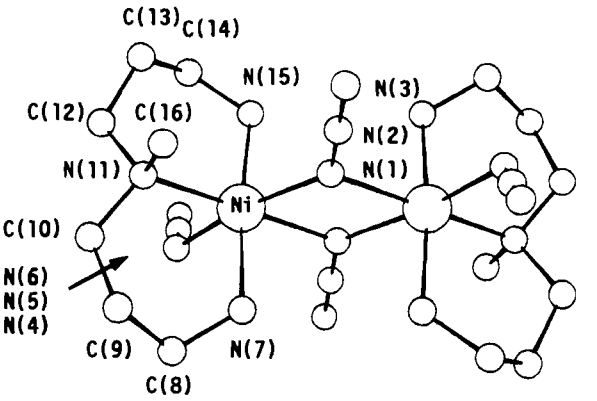

Figure 1. Atom labeled drawing of [{$Ni_2(Medpt)_2(N_3)_2$}(μ-$(N_3)_2$)] (**1**) at 293 K.

Table 4. Main Bond Lengths and Angles for [{$Ni_2(Medpt)_2(N_3)_2$}(μ-$(N_3)_2$)], **1**

	190.5 K	293 K
N(1)−Ni	2.217(4)	2.207(2)
N(1)′−Ni	2.169(4)	2.197(2)
N(4)−Ni	2.099(3)	2.087(2)
N(7)−Ni	2.082(3)	2.091(2)
N(11)−Ni	2.175(3)	2.190(2)
N(15)−Ni	2.084(3)	2.098(2)
N(1)−N(2)	1.196(5)	1.201(3)
N(2)−N(3)	1.149(5)	1.159(3)
Ni−Ni′	3.448(1)	3.470(1)
N(1)−Ni−N(1)′	76.3(1)	76.0(1)
Ni−N(1)−Ni	103.7(1)	104.0(1)
N(4)−Ni−N(1)	169.8(1)	169.7(1)
N(7)−Ni−N(1)	87.9(1)	87.6(1)
N(11)−Ni−N(1)	100.8(1)	100.7(1)
N(15)−Ni−N(1)	88.4(1)	88.5(1)
N(4)−Ni−N(1)′	93.6(1)	93.8(1)
N(7)−Ni−N(1)′	87.2(1)	87.1(1)
N(11)−Ni−N(1)′	176.3(1)	176.0(1)
N(15)−Ni−N(1)′	88.2(1)	88.6(1)
N(7)−Ni−N(4)	90.1(1)	90.3(1)
N(11)−Ni−N(4)	89.2(1)	89.4(1)
N(15)−Ni−N(4)	92.9(1)	92.9(1)
N(11)−Ni−N(7)	90.4(1)	90.6(1)
N(15)−Ni−N(7)	174.6(1)	174.8(1)
N(11)−Ni−N(15)	94.1(1)	93.6(1)
N(1)−N(2)−N(3)	179.1(4)	179.7(2)
Ni−N(1)−N(2)	135.5(3)	135.7(2)
Ni−N(4)−N(5)	123.6(3)	124.9(2)

Magnetic Measurements. The variable temperature magnetic susceptibility data were recorded for all compounds between 300−4 K. Compounds **1** and **2** are strongly ferromagnetically coupled and compound **3** shows a strong antiferromagnetic behavior. Complex **1** shows a magnetic transition between 150−120 K, and for this reason a more detailed study of the magnetic behavior was performed : on cooling, the $\chi_M T$ value increases continuously but a shape change of $\chi_M T$ value occurs between 150−120 K (Figure 2), reaching a maximum at ca 45 K with $\chi_M T = 3.45$ cm^3 mol^{-1} K. At low temperature the curve quickly decreases due to zero field splitting of nickel(II) and weak AF interdimer interactions. On heating between 4−300 K, the plot reaches the same $\chi_M T$ maximum at 45 K and then $\chi_M T$ decreases gradually to reach 2.80 cm^3 mol^{-1} K at room temperature. This magnetic transition seems not reversible, at least in the time of the measurement. Plots of magnetic data for compounds **2** and **3** are shown in Figure 3.

(23) Sheldrick, G. M. SHELX. A computer program for crystal structure determination. University of Cambridge, England, 1976.
(24) *International Tables for X-ray Crystallography*; Kynoch Press, Birmingham, England, 1974; Vol. IV, pp 99−110 and 149.

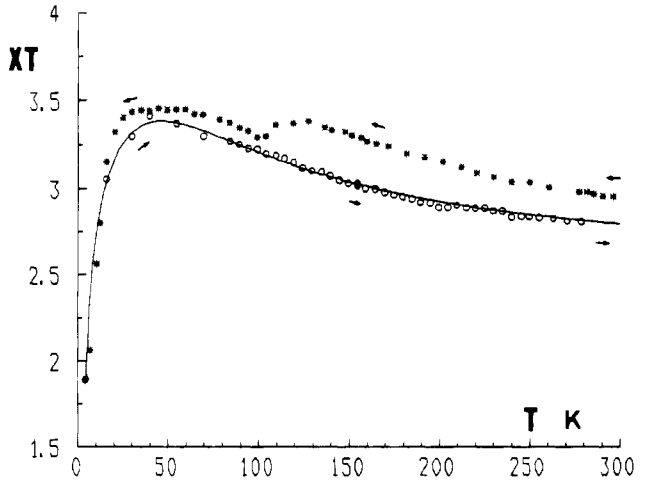

Figure 2. Molar magnetic susceptibility plots of a polycrystalline sample of [{$Ni_2(Medpt)_2(N_3)_2$}(μ-$(N_3)_2$)] (**1**) in the 300−4 K (*) and 4−300 K (O) range of temperatures. Solid line shows the best fit obtained (see text).

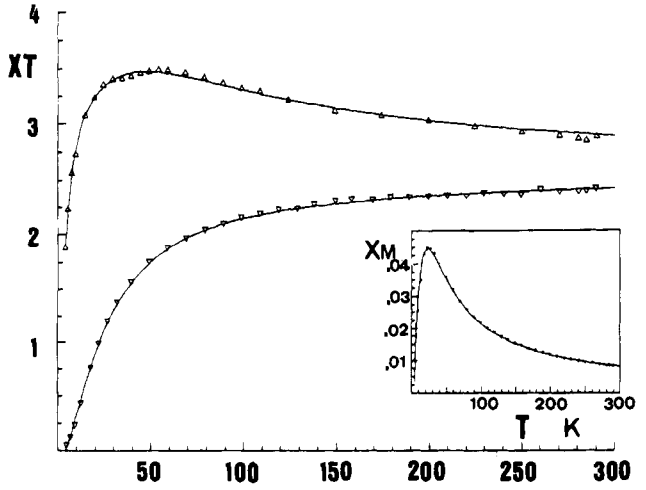

Figure 3. $\chi_M T$ *vs* T plots of a polycrystalline sample for [{$Ni_2(dpt)_2(N_3)_2$}(μ-$(N_3)_2$)] (**2**) and **3** (△ and ▽ respectively), in the 300−4 K range of temperatures. Inset, χ_M *vs* T plot for compound **3**. Solid lines show the best fits obtained.

The magnetic behavior of **2** is close to **1**: $\chi_M T$ at 300 K is 2.80 $cm^3\ mol^{-1}$ K, the maximum $\chi_M T$ value (3.41 $cm^3\ mol^{-1}$ K) is found at 54 K, and the final $\chi_M T$ value is 1.90 $cm^3\ mol^{-1}$ K at 4 K, whereas **3** shows a typical behavior of AF coupled dimer, with a maximum in the χ_M *vs* T plot at 22 K (Figure 3, inset).

The χ_M*T vs temperature curves of the dinuclear complexes **1** and **2** were least-squares fitted to the theoretical expression of the magnetic susceptibility given by Ginsberg et al.,[1] from the Hamiltonian

$$H = -2JS_1S_2 - D(S_{1z}^2 + S_{2z}^2) - g\beta H(S_1 + S_2) - z'S\langle S\rangle$$

in which J is the intradimer exchange parameter, D is the single ion zero-field splitting, z' is the effective interdimer exchange, and $g_x = g_y = g_z \equiv g$ is assumed. The resulting χ_M expression is

$$\chi_M = 2Ng^2\beta^2/3k[F_1/(T - 4z'F_1) + 2F'/(1 - 4z')]$$

where F_1 and F' are functions of temperature, zerofield splitting, and the intradimer exchange parameter J. It is interesting to point out that this expression gives accurate values of J and g, but D and z' parameters are not well determined from magnetic susceptibility data.[1] For compound **1** the data corresponding to the 300−4 K region cannot be accurately fitted due to the large errors that imply a fragmentary plot and consequently, only the 4−300 K experimental data have been treated. The best fitting parameters are $2J = 46.7\ cm^{-1}$, $g = 2.22$, $D = -5.04\ cm^{-1}$, $z' = -0.57\ cm^{-1}$, $R = 2.6 \times 10^{-5}$ for **1** and $2J = 49.3\ cm^{-1}$, $g = 2.25$, $D = -4.80\ cm^{-1}$, $z' = -0.56\ cm^{-1}$ and $R = 5.9 \times 10^{-5}$ for **2**. The minimized function was $R = \Sigma(\chi_M T^{calcd} - \chi_M T^{obs})^2/\Sigma(\chi_M T^{obs})^2$. These values indicate that the FM superexchange interaction is extremely effective and comparison with literature data for other nickel(II) dinuclear complexes with a μ-azido bridge,[9] shows that compounds **1** and **2** are placed between the most ferromagnetic μ-azido complexes reported to date.

Compound **3** was fitted by using the isotropic Hamiltonian $-2JS_AS_B$ ($S_A = S_B = 1$) to the expression[25]

$$\chi_M = (2N\beta^2g^2/kT)(2\exp(x) + 10\exp(3x))/(1 + 3\exp(x) + 5\exp(3x))$$

where N, β and k have the usual meanings and $x = J/kT$. The Ginsberg formula,[1] with zerofield splitting D, has not been considered since the effect of D at low temperatures can be neglected due to the large stabilization of the singlet ground state.

The best fit parameters are $2J = -16.7\ cm^{-1}$, $g = 2.30$, $R = 9.4{\cdot}10^{-4}$, where $R = \Sigma(\chi_M calcd - \chi_M obs)^2/\Sigma(\chi_M obs)^2$. On the basis of the magnetic susceptibility results, coordination of azido ligand for compounds **2** and **3** can be unambiguously assigned as end-on for **2** giving strong ferromagnetic coupling and end-to-end for **3** giving antiferromagnetic coupling.[10]

Magnetic Transition of [{$Ni_2(Medpt)_2(N_3)_2$}(μ-$(1,1\text{-}N_3)_2$)] (1). Magnetic Data. The magnetic data described above in the 300−4−300 K range indicate that after the transition in the 150−120 K interval, the process continues up to stabilization of the low-temperature form. After **1** is cooled at 4 K, the transition is not reversible when performs the increasing temperature measurement, but maintaining the compound at room temperature slowly returns to the original form in a few days. The χ_M and $\chi_M T$ *vs* temperature plots for an experiment in the 300−80−300 K range, in which the sample was maintained at 80 K for 30 min before the heating process, are shown in Figure 4a,b. The magnetic transition was observed between 125 and 115 K during the cooling measurement and between 175 and 185 K during the heating measurement. It is interesting to point out that the return points in the 80−115 K interval do not match with those in the decreasing 115−80 K interval, indicating the continuation of the process during the isothermal cooling. In these conditions, the hysteresis is observed in a wide range of temperature, close to 60°.

Experiments in which the temperature was held at 80 K for 2 h periods stabilize the low-temperature form (Figure 4c) during the increasing temperature measurement, indicating the strong dependence of the phenomenon with the thermal history of the compound.

Calorimetric Data. DSC analysis shows two sharp peaks at 279.3 K (−3.58 kcal mol^{-1}) and at 181.6 K (−9.14 kcal mol^{-1}) during the cooling measurement and also two peaks at 187.9 K (9.52 kcal mol^{-1}) and 281.8 K (3.52 kcal mol^{-1}) during the heating measurement, as shown in Figure 5. The two processes are reversible, indicating thermal hysteresis.

Powder X-ray Data. The X-ray powder diffraction studies were performed on the basis of the data provided by susceptibility and calorimetric measurements and before the resolution of the structure of **1** at low temperature. The sample was cooled

(25) O'Connor, C. J. *Prog. Inorg. Chem.* **1982**, *29*, 203.

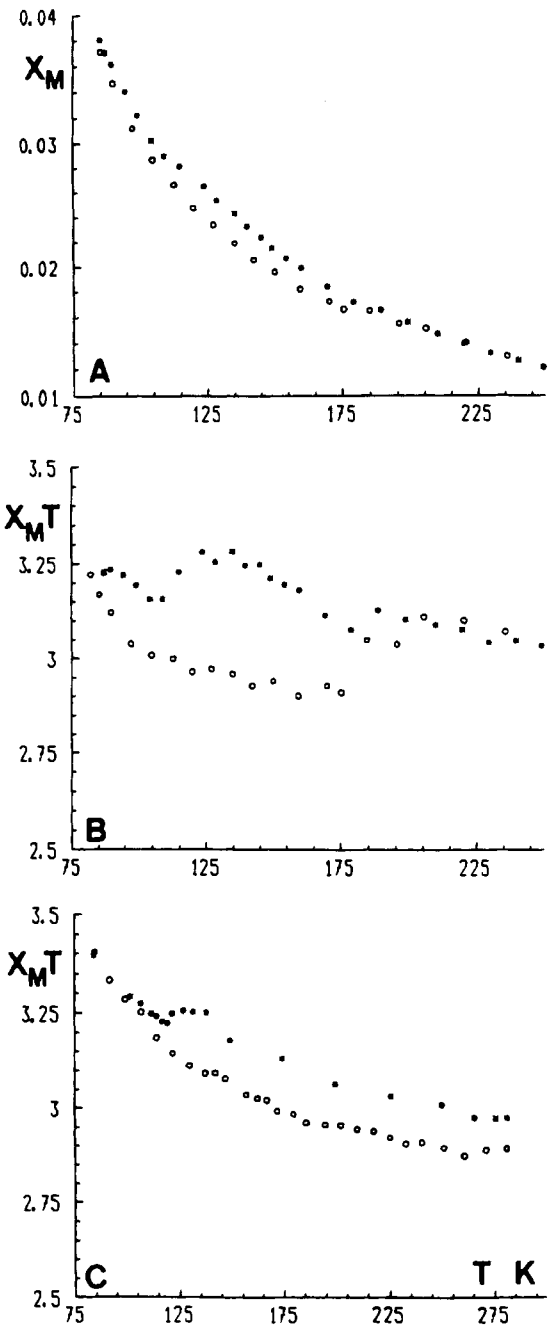

Figure 4. Magnetic susceptibility plots of a polycrystalline sample of $[\{Ni_2(Medpt)_2(N_3)_2\}(\mu\text{-}(N_3)_2)]$ (**1**) under different experimental conditions: (**A** and **B**) χ_M *vs* T and χ_MT *vs* T plots in the 250−80 K (*) and 80−250 K (O) ranges of temperatures, showing the reversibilyty of the magnetic transition. (C) χ_MT *vs* T plot in the 290−80 K (*) and 80−290 K (O) ranges of temperatures, maintaining the sample at 80 K for a long period. In this conditions the transition becomes stable and does not appear reversible.

in the 293−193 K range at 5° min^{-1}, leaving the compound at fixed temperature for 15 min before measurement, in order to stabilize the equipment and the sample. The comparison between the intensities collected at different temperatures shows a difference in the localization of the peaks attributable to dilatation processes. A broadening of the peaks was also observed at low temperatures (in the range indicated by the DSC measurements), which is reversible when the temperature increases. Measurements at 373 K show the decomposition of the compound.

The differences in the position and temperature range between the magnetic data and the remaining techniques is due to the fact that the susceptometer does not permit a constant rate of cooling/heating, and the response should be different in DSC and powder X-ray techniques.

Monocrystal X-ray Data. The above indicated measurements indicate that a structural transition occurs at low temperatures for **1** and, consequently, the determination of the structure was performed at 293 and 190.5 K under the previously indicated conditions. A view of the dinuclear entity at room temperature with its labeling scheme is shown in Figure 1. The view of the complex at low temperature is, in principle, indistinguishable. Effectively, the structures are very similar, as can be observed from Tables 1−3; most of the bond lengths and angles differ by less to three standard deviations. In both structures the nickel atom shows a distorted octahedral coordination, linked to three N_3^- ligands and the $C_7H_{19}N_3$ group. N(1), N(1)′, N(11), and N(4) atoms are in the equatorial plane in the two structures, with the nickel atom deviated 0.039(1)Å from the mean plane. Two N_3^- ligands act as a bridge between two nickel atoms in end-on fashion. A molecular symmetry center, which is also a crystallographic symmetry center, is present in the two isomers. The four-membered ring Ni_2N_2 is planar, while the 1,3-propanediamine moieties show a chair-conformation with C(13), C(9), and N(1) atoms out of the plane defined by the remaining four atoms. The most significant structural differences can be observed in the Ni_2N_2 four-membered ring defined by Ni(1), N(1), N(1)′, and Ni(1)′atoms. At 293 K the ring shows the following bond parameters: Ni(1)−N(1), 2.207(2) Å; Ni(1)−N(1)′, 2.197(2) Å; Ni(1)−N(1)−Ni(1)′, 104.0(1)°; N(1)−Ni(1)−N(1)′, 76.0(1)°; Ni(1)−Ni(1)′, 3.470(1) Å, whereas at 190.5 K these values are 2.217(4) Å, 2.169(4) Å, 103.7(1)°, 76.3(1)°, and 3.448(1) Å, respectively. These bond parameters are of the same order as those found in the three end-on nickel dimers reported to date.[9] From this analysis, the high-temperature structure shows a more symmetric Ni−N (bridge) bonding, whereas the low-temperature structure shows a more asymmetric bonding scheme; the Ni−N(1) and the Ni−Ni distances differ by 0.048 and 0.022 Å respectively. The remaining bond parameters are practically identical in the two structures. This asymmetrization is schematized in Figure 6. Thus, the variation in the magnetic properties should be attributed to the structural differences in the bridging fragment.

Discussion of the Asymmetrization. Taking into account the local symmetry of the dinuclear $Ni(N_3)_2Ni$ entities explained in the crystallographic part, the local point group symmetry can be assumed as D_{2h} (rhombic geometry) before the arrangement or asymmetrization. The molecular orbitals with the possibility of unpaired electrons (HOMO and LUMO) are $z^2 + z^2$ (a_g), $z^2 - z^2$ (b_{3u}), $xy + xy$ (b_{1g}) and $xy - xy$(b_{2u}), all partially delocalized over the nitrogen atoms of the ligand. Extended Hückel calculations carried out by means of the CACAO program[26] show that the $xy + xy$ (b_{1g}) molecular orbital is the most stable for any geometry square-planar or rhombic.

The necessary condition for ferromagnetic coupling is the degeneracy of the molecular orbitals[27] derived from the symmetric and antisymmetric combinations of the accidental orthogonal magnetic orbitals. Taking into account the ferromagnetic behavior derived from the experimental measurements we must assume that the molecular orbitals b_{3u} and a_g are almost degenerate, like b_{1g} and b_{2u}, respectively. At room temperature the population of these four molecular orbitals is almost random and the χ_MT value is close to that expected for two Ni(II) independent $S = 1$ ions. When temperature decreases the

(26) Mealli, C.; Proserpio, D. M. *J. Chem. Educ.* **1990**, *67*, 3399. The CACAO program was kindly supplied by Prof. Mealli.
(27) Hay, P. J.; Thibeault, J. C.; Hoffmann, R. *J. Am. Chem. Soc.* **1975**, *97*, 4884.

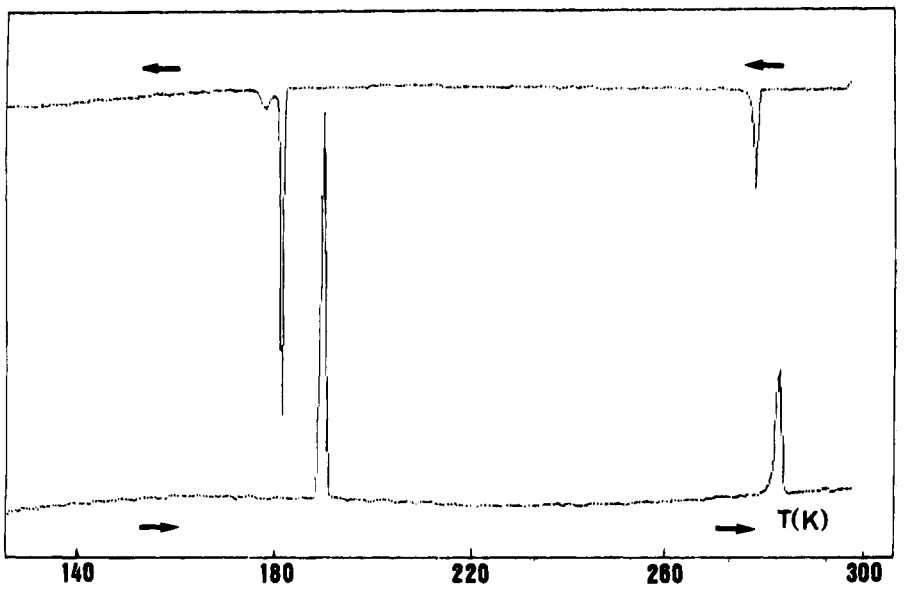

Figure 5. DSC measurement for $[\{Ni_2(Medpt)_2(N_3)_2\}(\mu\text{-}(N_3)_2)]$ showing the thermal hysteresis between 181.6 and 187.9 K.

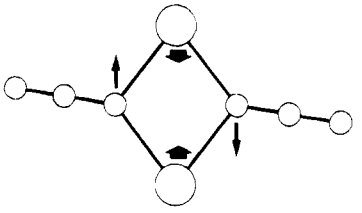

Figure 6. Positional changes in the Ni_2N_2 core of $[\{Ni_2(Medpt)_2(N_3)_2\}(\mu\text{-}(N_3)_2)]$ during the high–low temperature transition.

ground state $S = 2$ becomes more and more populated: at this moment the four electrons are correlated and the ferromagnetic term in the Hamiltonian tends to align these electrons in a parallel way. This correlation may be geometrically very important if we consider the transition density $\Phi_1{}^*\Phi_2$ where Φ_1 and Φ_2 are the corresponding molecular orbitals. To determine when this effect may be important we need only to consider the symmetry species of this transition density $\Phi_1{}^*\Phi_2$. If one of these direct products corresponds to a normal vibrational mode of the molecule, then a second-order Jahn–Teller distortion is possible.[28] In this regard the relative energies of these orbitals are irrelevant. In any case they are very close in energy, with a temperature-dependent occupancy, and thus the second-order Jahn–Teller effect is operative.

By means of group theory the symmetry labels of the stretchings and bendings in $Ni(N_3)_2Ni$ entities are as follows: $A_g + B_{1g} + B_{2u} + B_{3u}$ (stretchings) and $A_g + B_{1u}$ (bendings). Correlating the electrons in their molecular orbitals, we can see that the direct product between b_{1g} (xy + xy) and a_g ($z^2 + z^2$) or between b_{3u} ($z^2 - z^2$) and b_{2u} ($xy - xy$) is B_{1g}, which corresponds exactly to the geometrical rearrangement or asymmetrization which takes place in the phase transition a low temperature (Figure 6).

Finally, it must be pointed out that the second-order Jahn–Teller effect takes place because the symmetry is lowered due to the possibility of a mixing between two molecular orbitals of the same symmetry after the distortion: one is stabilized and the other is destabilized. From magnetic point of view this fact means that a small gap between these molecular orbitals has been introduced, giving a net antiferromagnetic contribution (J_{AF}) which tends to counteract the ferromagnetic contribution (J_F). Thus, it is likely that after the phase transition the ferromagnetic behavior is less pronounced than before the transition, as is experimentally observed (Figures 2 and 4). Similar behavior, although less marked, has been observed in other series of dinuclear Ni(II) complexes with two 1,1-azido bridging ligands.[29]

Acknowledgment. Financial assistance from CICYT (Grant PB93/0772) is acknowledged.

Supplementary Material Available: Text detailing the X-ray structure determination and tables giving crystal data and details of the structure determination, atom coordinates, bond lengths, bond angles, anisotropic thermal parameters, and hydrogen atom locations (8 pages). Ordering information is given on any current masthead page.

IC940359M

(28) For a description of the second-order Jahn–Teller effect see, e.g.: Burdett, J. K. *Molecular Shapes*; Wiley: New York 1980.

(29) Bastos, C.; Thesis, Departament de Química Inorgànica, Universitat de Barcelona, 1991.